Pergamon

Int. J. Solids Structures Vol. 34, Nos. 35–36, pp. 4449–4461, 1997

0020–7683/97 $17.00 + .00

PII: S0020–7683(97)00052–8

DETERMINATION OF ALL STRESS COMPONENTS FROM MEASUREMENTS OF THE STRESS INVARIANT BY THE THERMOELASTIC STRESS METHOD

Y. MURAKAMI
Department of Mechanical Science and Engineering, Faculty of Engineering, Kyushu University, Hakozaki, Fukuoka, 812-81 Japan

and

M. YOSHIMURA
JEOL Creative Co. Ltd., Musashino, Shojima, Tokyo, 196 Japan

(*Received* 10 *June* 1996; *in revised form* 5 *February* 1997)

Abstract—A method for the resolution of all stress components from the first invariant J_1 measured by thermoelastic stress analyzer is described. This method may be used to determine, not only surface stress, but also internal stress and stress on the underside.

The method is based on the following procedure:

(1) Pick an arbitrary domain Ω, within the structure, for which the stresses are required.
(2) Measure J_1 on the surface of Ω.
(3) Determine the optimum traction along the boundary Γ, which is a part of Ω, by the least squares method such that the difference between the measured J_1 and the calculated J_1 is at a minimum. Either FEM or BEM may be used for this calculation.

Examples of stress resolution for a two-dimensional stress concentration problem and a three-dimensional stress concentration problem are shown. The accuracy of the stress resolution is discussed. © 1997 Elsevier Science Ltd.

1. INTRODUCTION

Since the development of the thermoelastic stress analyzer, it has been used by many industries and researchers for nondestructive experimental stress analysis. Although the basic principle of thermoelastic effect was established in the 19th century (Weber, 1830; Thomson, 1853; Thomson, 1878; Compton and Webster 1915), it is only recent developments in sensing technology that have permitted the practical application of the method. Due to the practical usefulness, more than 200 papers on the thermoelastic stress analysis and the analyzer have been published (Belgen, 1967; Jordon and Sandor, 1978; Mountain and Webber, 1978; Blanc and Giacommetti, 1981; Baker and Webber, 1982; Cox *et al.*, 1982; Nishimura *et al.*, 1984; Archer and Razdan, 1985; Rowe 1985; Sarihan *et al.*, 1985; Stanley and Chan, 1985; Cummings and Harwood, 1985; Mckelvie, 1986; Ishida *et al.*, 1986; Machin *et al.*, 1987; Rowlands, 1987; Shiratori *et al.*, 1987; Oliver, 1988; Kageyama *et al.*, 1988; Kitsunai *et al.*, 1994, and others). However, it has been pointed out that it is impossible in principle to determine all stress components by thermoelastic analysis because only the stress invariant of the first order is measured by this method. It has also been pointed out that only the stress invariant at surface can be determined. These two disadvantages of thermoelastic stress analysis have been thought to be fundamental in principle and unavoidable. Literature treating this method typically describes only the measured data (stress invariant) and the extended application to new materials and structures.

In this paper, a method which enables not only the resolution of all stress components from the measured stress invariant at surface, but also the determination of all stress components within the structure, is proposed. The method is based on a combination of

thermoelastic stress analysis and numerical stress analysis. If this method is established, the usefulness and applicability of the thermoelastic stress analyzer will be remarkably extended.

However, there exist some problems which cannot be solved by this proposed method. It will be shown in Appendix A that such problems are trivial and the proposed method is applicable to most practically important problems.

2. BASIC PRINCIPLE OF THERMOELASTIC STRESS ANALYSIS

The temperature of a gas increases by adiabatic compression and decreases by adiabatic expansion. Solids behave in a similar manner to gases when subjected to instantaneous compression and tension. This phenomenon is called the thermoelastic effect. Within the elastic deformation of isotropic solids without initial stress, dilatation or contraction (volume change) corresponds to the strain invariant of the first order I_1 $(= \varepsilon_x+\varepsilon_y+\varepsilon_z = \varepsilon_1+\varepsilon_2+\varepsilon_3 = \cdots)$. Based on Hooke's law, I_1 is correlated with the stress invariant of the first order J_1 $(= \sigma_x+\sigma_y+\sigma_z = \sigma_1+\sigma_2+\sigma_3 = \cdots)$. Thus, the heat generation in the elastic range of deformation of an elastic body under adiabatic loading can be proportionally correlated with J_1 and the relationship is given by;

$$\Delta T = -kTJ_1 \tag{1}$$

where ΔT = temperature change, k = thermoelastic coefficient, T = absolute temperature °K, J_1 = the stress invariant of the first order. k is determined from;

$$k = \alpha V_0/C_V \tag{2}$$

where, α: coefficient of thermal expansion, V_0: molar volume, C_V: molar heat at constant volume.

Thus, J_1 can be determined by the accurate measurement of ΔT.

The thermoelastic stress analyzer used in the measurement in this study was JTG-8000. Table 1 shows the main specifications of JTG–8000.

3. METHOD OF STRESS COMPONENT RESOLUTION

In order to explain the basic principle of stress component resolution from the measured values of stress invariant, consider a two-dimensional plane stress problem.

Table 1. Main specifications of JTG-8000

Stress measurement range	$-2{,}000$–$2{,}000$ N/mm^2 ($-5°$–$5°$)*[1]
Stress resolvability	0.4 N/mm^2 (0.001°)†
Measurable frequency	0.5–90 Hz
Angle of view	Horizontal 30°, Vertical 28°
Horizontal resolution	Over 300 lines (1.7 m rad)
Number of display dot	Horizontal 512 × Vertical 480
Data memories	512 × 480 × 32 bit 2 pages
Auto focus	Auto focus by thermo-signal
Visualization system	Display system with the identical axis and field view with thermo-image
Focal range	20 cm–∞ in front of camera
Measure wavelength	8–13 mm
Infrared detector	HgCdTe
Liquid nitrogen cooling	Over 6 hours

† In case of aluminum

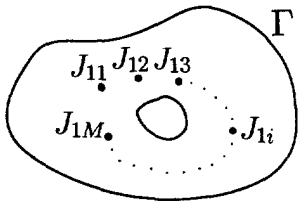

Fig. 1. Measurement of J_1.

Figure 1 shows a plate containing a hole. Assume that this plate is fixed along part of its boundary Γ and is subject to external loading along another part of Γ. Thus, we suppose the shape of the plate is known but the load boundary conditions are unknown.

We measure by thermoelastic stress analysis the stress invariant, J_1 of the first order at M points on the surface of this plate. We denote J_1 at point i ($i = 1 \sim M$) by J_{1i}. If we can determine the load boundary condition from the measured values of J_{1i}, we can determine all stress components at any point inside the plate by numerical stress analysis such as FEM and BEM. The procedure to determine the load boundary conditions follows.

As shown in Fig. 2, choose sufficient points along the boundary Γ. A unit normal force and then a unit tangential force is applied to each point in turn (from $j = 1$ to $j = N$). There is no definite rule to choose the N points along Γ. However, it is clear that the N points must be chosen so that they fairly reflect the boundary condition.

The next step is to calculate the value of stress invariant J^*_{1ij} at point i produced by the unit force at point j.

The true boundary condition P_j along Γ should make the following difference zero.

$$e_i = J_{1i} - \sum_{j=1}^{N} J^*_{1ij} P_j, \quad i = 1 \sim M, j = 1 \sim N. \tag{3}$$

To find the optimum values of P_j in a rational way, we apply the least square method to e_i. We define S as the sum of e_i^2 by

$$S = \sum_{i=1}^{M} (e_i^2). \tag{4}$$

Thus, the optimum values of P_j must satisfy

$$\frac{\partial S}{\partial P_j} = 0. \tag{5}$$

Equation (5) is a set of N linear simultaneous equations. Solving it, we can determine P_j ($j = 1 \sim N$).

Once the values P_j are determined we can calculate the stress components at any point on the plate by superimposing the stress components induced by P_j along Γ. For the

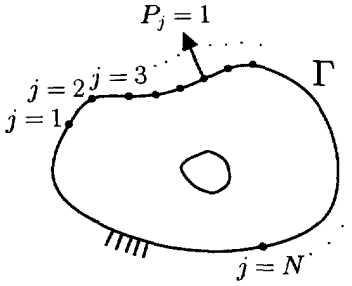

Fig. 2. Application of unit traction along boundary.

calculation of J^*_{1ij}, FEM or BEM may be used. It has been noted that choosing M and N such that they satisfy the relationship $M > 2N$, obtains the best results.

In the above example, we assumed that the shape of the plate was known before analysis. However, in practical applications the complete shape of the structure is not necessarily needed. We only need concern ourselves with the local domain Ω where the thermoelastic stress analysis will be made and define the boundary Γ of Ω inside which we apply the above method. This characteristic of the present method is practically very important, because we do not need to analyze a whole structure by FEM or BEM using a powerful computer.

There is no substantial difference between 2D and 3D analysis in the present method. Only the software of FEM or BEM may be changed. In other words, we need the information of the stress invariant on surface and the geometry of the structure in question. If the problem in question is not a trivial one as indicated in Appendix A (Fig. A1), the interior stress components in a 3D body can be determined only from the information of the stress invariant on surface and the known geometry. This will be demonstrated in Section 4.2.

The problems which are expected to be solved by the method proposed in this paper are essentially inverse problems. Analyzing inverse problems, we must always pay attention to instabilities of the solutions (Bui, 1993). However, if we can include in a structure in question one or more boundaries at which the boundary conditions can be well defined, the stability of the solution as the inverse problem can be much improved (this is the key point of the proposed method), though the accuracy and spatial information of data and number of data points still influence the stabilities.

4. APPLICATIONS

4.1. *A circular hole in an infinite plate under remote tension*

To verify the validity of the proposed method and examine the accuracy of the numerical calculation, we first solve a problem for which an exact solution is known.

Figure 3 shows an infinite plate containing a circular hole with radius a. The plate is subjected to a remote tension, $\sigma_x = \sigma_0$, $\sigma_y = 0$ and $\tau_{xy} = 0$ at infinity. The exact solution of this problem is given by Kirsch (1898) as follows.

$$\sigma_r = \frac{\sigma_0}{2}\left(1-\frac{a^2}{r^2}\right)-\frac{\sigma_0}{2}\left(1+\frac{3a^4}{r^4}-\frac{4a^2}{r^2}\right)\cos 2\theta$$

$$\sigma_\theta = \frac{\sigma_0}{2}\left(1+\frac{a^2}{r^2}\right)+\frac{\sigma_0}{2}\left(1+\frac{3a^4}{r^4}\right)\cos 2\theta$$

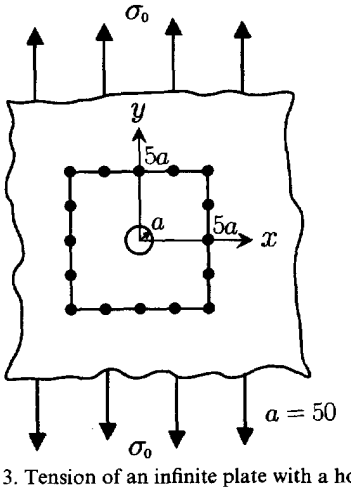

Fig. 3. Tension of an infinite plate with a hole.

Table 2. Analytical results of Fig. 3

(x, y) [mm]	J_1		σ_x/σ_0		σ_y/σ_0		τ_{xy}/σ_0	
	Exact	Cal.	Exact	Cal.	Exact	Cal.	Exact	Cal.
(60, 0)	2.3889	2.3890	0.3183	0.3191	2.0706	2.0699	0	0.0000
(70, 0)	2.0204	2.0203	0.3748	0.3725	1.6456	1.6478	0	0.0000
(80, 0)	1.7813	1.7812	0.3571	0.3540	1.4242	1.4271	0	0.0001
(0, 70)	−0.0204	−0.0204	−0.1354	−0.1411	0.1150	0.1207	0	0.0000
(60, 30)	1.6667	1.6667	0.1407	0.1335	1.5259	1.5332	−0.1333	−0.1299

Exact: Exact solution Cal.: Calculated stress

$$\tau_{r\theta} = \frac{\sigma_0}{2}\left(1 - \frac{3a^4}{r^4} + \frac{2a^2}{r^2}\right)\sin 2\theta \tag{6}$$

where r and θ are the polar coordinates (r, θ) with the angle θ measured from x axis.

The domain Ω is defined by a square region with a side length $5a$.

A side of the square region is divided into 4 points which are selected for the application of external load. The external unit loads along Γ are applied so that they vary linearly from zero to unity value between two neighboring points. This way of distribution of loads is commonly used in the boundary element method (BEM), i.e. the unit load in this case is defined so that the load is continuously distributed between 3 neighboring discretized points and the magnitude of force at the midpoint is unit and the magnitude between the midpoint and the two neighboring points at both sides decreases linearly from unit to zero.

The stresses inside Ω were calculated using BEM software (Hirai, 1984).

Instead of measuring the stress invariant J_1 using the thermoelastic stress analyzer, we obtain the sum $\sigma_r+\sigma_\theta$ at 56 points inside Ω from eqn (6) to give the values J_{1i}. Table 4 in Appendix B shows coordinates of the selected points for J_{1i}.

The details of calculation of this problem are explained in Appendix B.

Table 2 compares the exact values of J_1 $(= \sigma_r+\sigma_\theta)$ and the calculated values by the proposed method. Since in this case, we know the exact solution for all stress components (eqn 6), we can compare not only J_1 but also the exact values of stress components and the calculated values. The agreement between the exact values and the calculated values is very good.

The accuracy of the determination of all stress components σ_r, σ_θ and $\tau_{r\theta}$ is approximately of the same order as the accuracy of that of J_1 $(= \sigma_r+\sigma_\theta)$ determined by the analysis.

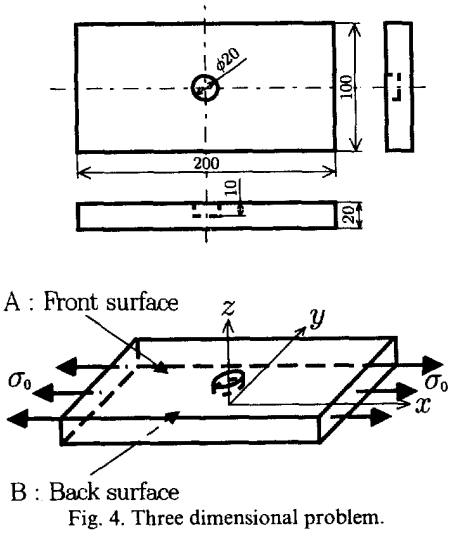

Fig. 4. Three dimensional problem.

This implies that even if the measured values of J_1 are exact, the results of numerical analyses always include some errors due to the analytical modeling.

4.2. *Tension of a rectangular plate containing a part-through cylindrical hole (3D problem)*

Figure 4 illustrates the shape and loading of the problem. This is a 3-D problem. A hole in the center of the plate does not penetrate the plate. We first measured the temperature change ΔT on the front surface including the base of the cylindrical hole and determined J_1. From the measured values of J_1, we determined the stresses on the back surface.

As a second problem, we measured the temperature change ΔT, on the back surface and, accordingly, J_1. From the data J_1 on the back surface, we determined the stresses on the front surface and back surface.

4.2.1. *Determination of stresses from the measurement of temperature change on the front surface (surface A in Fig. 4).* Figure 5 shows the image measured by the thermoelastic stress analyzer. Table 3 shows the results of calculation. The stress analysis was carried out using FEM software with tetrahedral constant strain elements. Considering the symmetry of the specimen shape, only one quarter was analyzed. The number of elements was 5033 and nodes 1196. The mesh pattern is shown in Appendix C. The error of the analytical value of J_1 to the measured values is less than 10%. However, the analytical error is always dependent both on the measured values of J_1 and the method of analysis itself. It is shown in Appendix D that if we use a smaller specimen, the error tends to increase. If the size of the structure in question is too small and the stress gradient at the stress concentration is very large, then the measured values cannot reflect exactly the steep variation of stress because of spatial resolution limitations of the analyzer.

4.2.2. *Determination of stresses from the measurement of temperature change on the back surface (surface B in Fig. 4).* If only the stress invariant J_1 on the surface where we measure the temperature change ΔT can be determined by the thermoelastic stress analysis method, the usefulness is limited. To verify that the proposed method enables one to overcome this difficulty, we now determine the stresses on the opposite side to the measurement.

Figure 6 shows the image of the measurement on surface B in Fig. 4. We are interested in the stress concentration in the vicinity of the hole on surface A.

Figure 7 compares the measured and calculated values. The symbol ○ shows the distribution of the values J_1 experimentally measured on surface A and the symbol ■ shows the calculated values of J_1 at the same points. The symbol ▲ is the values of J_1 at the same points as ○ on surface A calculated using the measurement on surface B. Although the accuracy of the latter values is a somewhat poorer than those calculated using the data on surface A, it is still satisfactory for most practical applications.

Figure 8 shows the comparison between the measurement and calculation on surface B. The symbol ○ is the measurement of J_1, ■ the calculated values based on the measurement on surface A (Fig. 5) and ▲ the calculated values based on the measurement on surface B (Fig. 6).

Table 3. Analytical results of Fig. 4 [MPa]

(x, y, z) [mm]	J_1		σ_x	σ_y	σ_z
	Meas.	Cal.	Cal.	Cal.	Cal.
(1.250, 17.500, 19.722)	32.2	30.7	25.9	4.7	0.2
(1.250, 37.500, 19.722)	24.4	24.8	23.5	1.3	−0.1
(8.650, 10.625, 19.722)	23.9	24.4	22.5	0.6	1.3
(3.750, 7.160, 9.688)	29.4	29.1	26.8	1.8	0.5
(0.625, 1.875, 9.688)	27.2	24.9	23.7	1.2	0.0

Meas.: Measured stress Cal.: Calculated stress

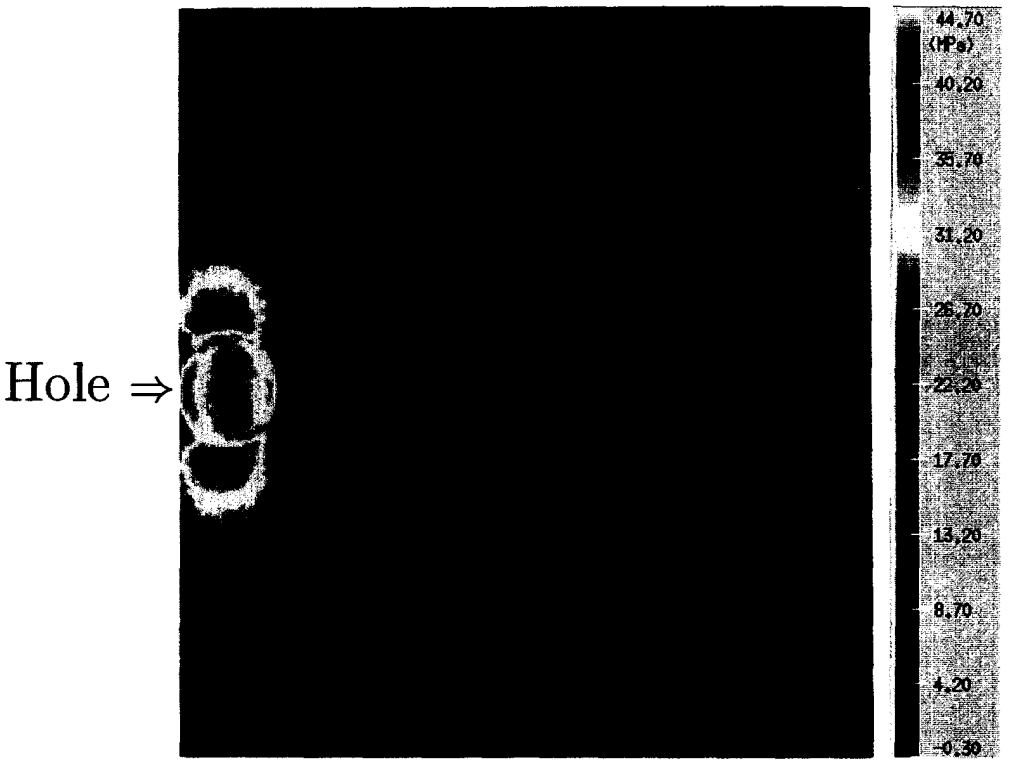

Fig. 5. Thermoelastic image analysis on front surface A of Fig. 4.

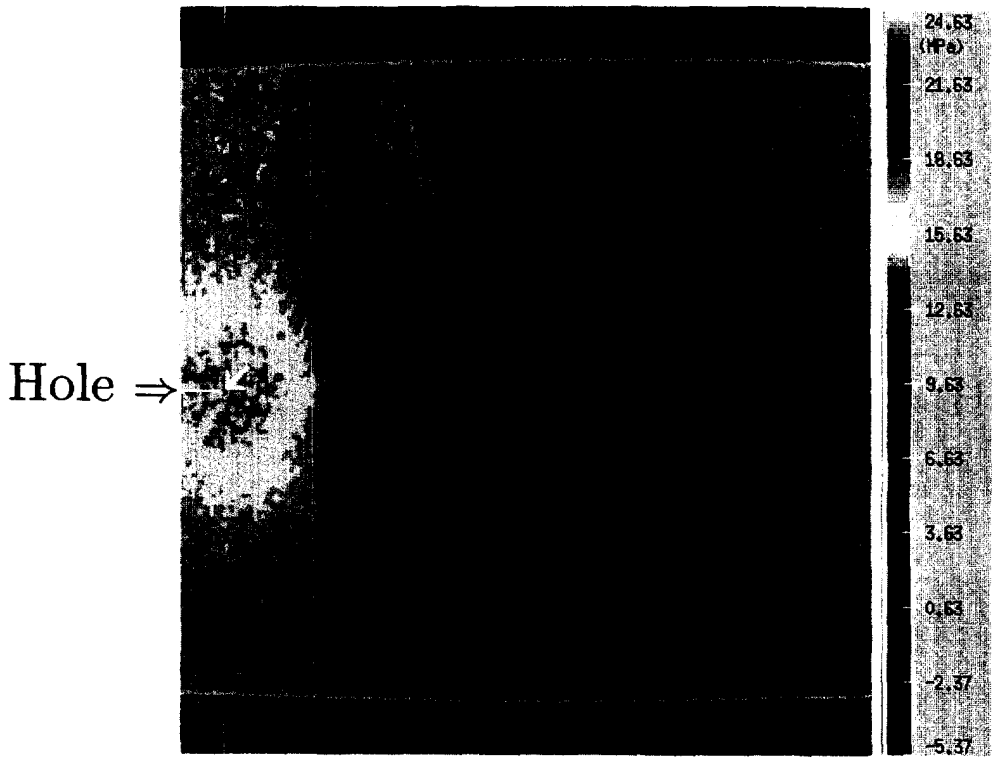

Fig. 6. Thermoelastic image analysis on back surface B of Fig. 4.

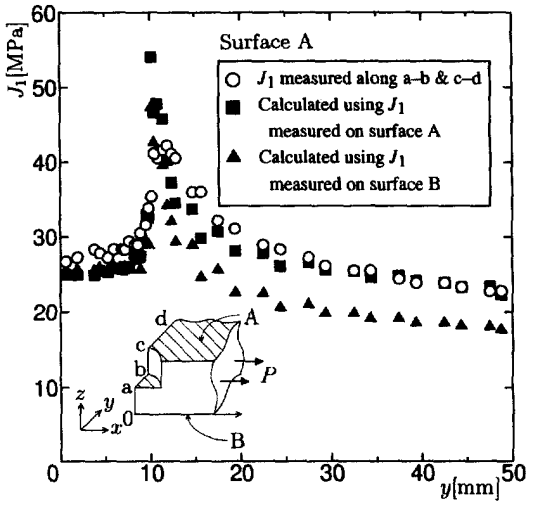

Fig. 7. Distribution of stress invariant J_1 of surface elements along a–b and c–d on surface A. a–b = 10 mm.

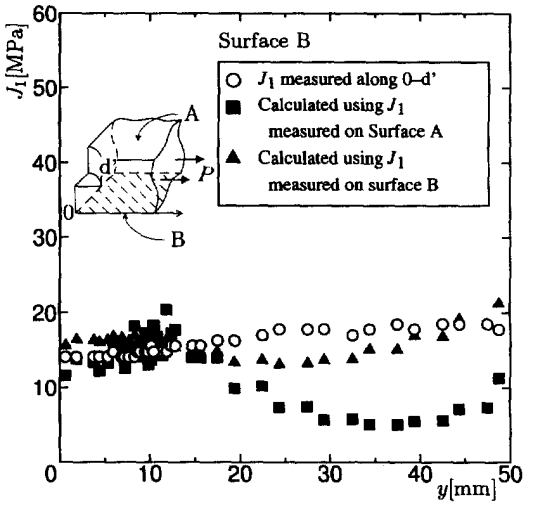

Fig. 8. Distribution of stress invariant J_1 of surface elements along 0–d' on surface B.

5. CONCLUSION

In the past, the following two disadvantages for thermoelastic stress analysis have been pointed out.

(1) Only the stress invariant of the first order J_1 $(= \sigma_x+\sigma_y+\sigma_z = \sigma_1+\sigma_2+\sigma_3 = \cdots)$ can be measured and the resolution of all stress components was thought to be impossible in principle.
(2) Only the information on the surface can be obtained.

In the present paper, a method to overcome both these disadvantages has been developed. The conclusions are summarized in the following.

(a) The basic conditions which enables one to resolve all stress components are theoretically made clear. Most practical problems can be solved by the application of the proposed method. Although there exist some problems which cannot be solved by the proposed method, such problems are of little practical importance.
(b) By the application of the proposed method to a two-dimensional stress concentration problem whose exact solution is known, the validity and accuracy of the proposed method has been verified.

(c) Based on the measurement on a 3D stress concentration problem, the validity of the complete resolution of a 3D problem has been verified. Moreover, the determination of the stress within and on the back face of the specimen was also shown. By the proposed method, the capability of the thermoelastic stress analysis technique and its practical value have been substantially extended.

Acknowledgements—The authors thank Prof. T. Mura of Northwestern University, Prof. R. A. Smith and Dr R. S. Dwyer-Joyce of University Sheffield, Dr T. Sakai of TOYOTA MOTOR Corp. and Dr A. Blarasin of CENTRO RICERCHE FIAT for their useful discussion on this paper.

REFERENCES

Archer, R. and Razdan, D. (1985) Stress analysis of railway coach body panels by means of the SPATE technique. In *Proceedings of the SEM Spring Conference on Experimental Mechanics*, Las Vegas, Nevada, pp. 740–746.

Baker, L. R. and Webber, J. M. B. (1982) Thermoelastic stress analysis. *Optica Acta*, **29**, 555–563.

Belgen, M. H. (1967) Infrared radiometric stress instrumentation application range study. *NASA Report CR-1067*.

Blanc, R. H. and Giacommetti, E. (1981) Infrared stroboscope—a method for the study of thermomechanical behaviour of materials and structures at high rates of strain. *International Journal of Solids and Structures*, **17**, 531–540.

Bui, H. D. (1993) *Introduction aux problémes inverses en mécanique des matériaux*. Direction des études et recherches d'électricité de France.

Compton, K. T. and Webster, D. B. (1915) Temperature changes accompanying the adiabatic compression of steel. Verification of W. Thomson's theory to a very high accuracy. *Physics Review, Ser.* 2, **5**, 159–166.

Cox, L. J., Holbourn, P. E., Oliver, D. E. and Webber, J. M. B. (1982) Stress analysis of complex structures using the thermo-elastic effects. In *Proceedings of the 7th International Conference on Experimental Stress Analysis*, Haifa, Israel, pp. 538–544.

Cummings, W. M. and Harwood, N. (1985) Thermoelastic stress analysis under broadband random loading. In *Proceedings of SEM Spring Conference on Experimental Mechanics*, Las Vegas, Nevada, pp. 844–850.

Hirai, T. (1984) *Elastic Stress Analysis Programs and Its Applications*, Vol. 1. Rikotosho, Tokyo.

Ishida, Y., Nishimura, S., Hatakenaka, M. and Teramoto, M. (1986) Development of Nissan's new twin-cam engine series. *Internal Combustion Engine*, **25**, 25–40.

Jordon, E. H. and Sandor, B. I. (1978) Stress analysis from temperature data. *Journal of Testing and Evaluation*, **6**, 325–331.

Kageyama, K., Ueki, K. and Kikuchi, M. (1988) Thermoelastic technique applied to stress analysis of carbon fiber reinforced composite materials. In *Proceedings of the VI International Congress on Experimental Mechanics*, Portland, OR, pp. 931–936.

Kirsch, G. (1898) *VDI-Z*, **42**, 797–807.

Kitsunai, Y., Sasaki, T. and Honda, T. (1994) Determination of stress concentration factors for notched specimens by means of infrared method and fatigue crack initiation life. *Japan Society of Mechanical Engineers* (preprint), No. 940-37 B, pp. 58–59.

Machin, A. S., Sparrow, J. G. and Stimson, M. G. (1987) Mean stress dependence of the thermoelastic constant. *Strain*, **23**, 27–30.

McKelvie, J. (1986) Some practical limits to the applicability of the thermoelastic effect. In *Proceedings of the VIIIth International Conference on Experimental Stress Analysis*. Martinus Nijhoff Publishers, Amsterdam, pp. 507–518.

Mountain, D. S. and Webber, J. M. B. (1978) Stress pattern analysis by thermal emission (SPATE). In *Proceedings of the Society of Photo-optics Institute of Engineers*, **164**, 189–196.

Nishimura, M., Yuasa, M. and Suzuki, K. (1984) On stress concentration in structures (1st report: stress measurement by thermal emission). *Journal of the Society of Naval Architects of Japan*, **155**, 316–323.

Oliver, D. E. (1988) Vibration pattern imaging with SPATE. In *Proceedings of the VI International Congress on Experimental Mechanics*, Portland, OR, pp. 830–835.

Rowe, W. J. (1985) Thermal conductivity measurement with a scanning radiometer. In *Proceedings of the SEM Spring Conference on Experimental Mechanics*, Las Vegas, Nevada, pp. 723–728.

Rowlands, R. E. (1987) Photomechanical analysis of composite and other materials. *SPIE*, San Diego.

Sarihan, V., Oliver, D. and Russell, S. S. (1985) Thermoelastic stress analysis of an automobile engine connecting rod. In *Proceedings of the SEM Spring Conference on Experimental Mechanics*, Las Vegas, Nevada, pp. 729–739.

Shiratori, M., Miyoshi, T., Maruyama, A. and Nakanishi, T. (1987) Measurement of stress intensity factor, K, and J-integral for cracked members by a scanning infrared camera. *Transactions of the Japan Society of Mechanical Engineers A*, **53**, 1699–1705.

Stanley, P. and Chan, W. K. (1985) SPATE studies of the stress distributions in steel plates and rings under in-plane loading. In *Proceedings of the SEM Spring Conference on Experimental Mechanics*, Las Vegas, Nevada, pp. 747–757.

Thomson, W. (1853) On the dynamical theory of heat. *Transactions of the Royal Society*, **20**, 261–283.

Thomson, W. (1878) On the thermoelastic thermomagnetic and pyro-electric properties of matter. *Philosophical Magazine*, **5**, 4–27.

Timoshenko, S. P. and Goodier, J. N. (1982) *Theory of Elasticity*, 3rd edition, p. 178. McGraw-Hill Int., London.

Weber, W. (1830) Uber die specifisch Warmefester Korper insbesondere der Metalle. *Ann d. Physik u. Chemie* 1830, **96**, 177–213.

APPENDIX A

In the main text of this paper, stress resolution has been shown to be possible and solvable examples have been described. However, there exist some problems which cannot be solved in principle.

For example, we can not distinguish, solely on the basis of J_1 information, problem A in Fig. A1(a) from problem C (Fig. A1(c)) which is made by the superposition of problems A and B (Fig. A1(b)), because the stress invariant J_1 of problem C is constant everywhere and completely identical to that of problem A. Therefore, so long as we measure J_1 on a region of the surface of a cylindrical bar of problems A and C, it is impossible to resolve all stress components.

Now, let us seek a method to distinguish such two problems from the viewpoint of two-dimensional stress functions. In planar problems, the Airy stress function can be expressed with two analytical complex functions $\psi(z)$ and $\chi(z)$ in the following form (Timoshenko and Goodier, 1982).

$$\phi = \mathrm{Re}\,[\bar{z}\psi(z)+\chi(z)] \tag{A1}$$

where $z = x+iy$.

Using these complex stress functions, stresses are given by

$$J_1 = \sigma_x+\sigma_y = 4\,\mathrm{Re}\,\psi'(z) \tag{A2}$$

$$\sigma_y-\sigma_x+2i\tau_{xy} = 2\,[\bar{z}\psi''(z)+\chi''(z)] \tag{A3}$$

Equation (A2) indicates that J_1 depends on only $\psi(z)$. Thus, we cannot determine all stress components from only $\psi(z)$. The necessary condition to determine both $\psi(z)$ and $\chi(z)$ is information on τ_{xy}. This information cannot be obtained from the value of J_1 on the surface (compare problems D and E in Fig. A1). However, if we add the boundary condition along the circumference of the rectangular plates of problems D and E in Fig. A1 to the information on J_1 on the plate surface, we can determine the solution uniquely, because we have two conditions of eqns (A2) and (A3) at the boundary.

Thus, we conclude that the necessary and sufficient condition to determine all stress components from the information on the stress invariant of the first order J_1, is to choose the analytical boundary Γ such that it includes at least a boundary where the stress boundary conditions are known.

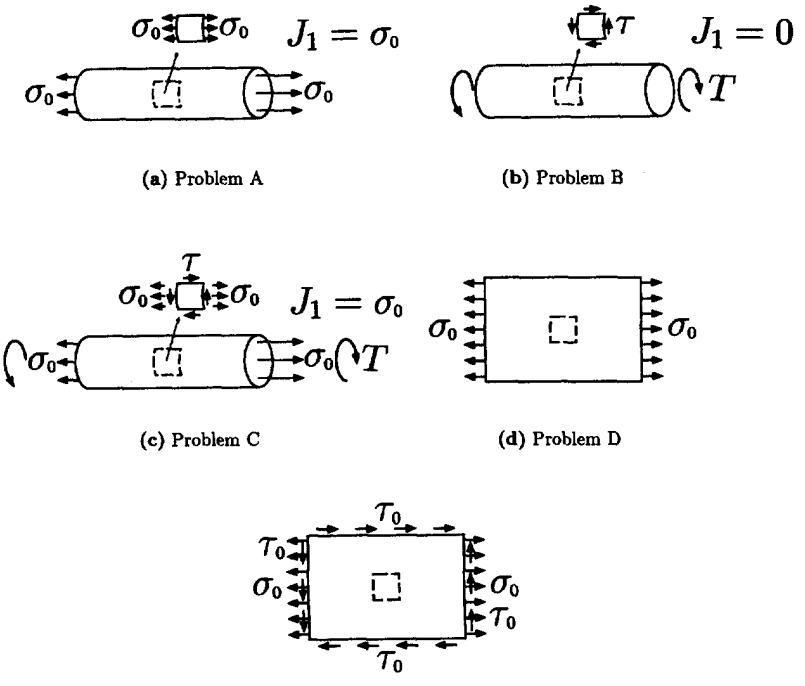

(a) Problem A (b) Problem B

(c) Problem C (d) Problem D

(e) Problem E

Fig. A1. Since $J_1 = 0$ in Problem B, J_1 in Problem C is identical to that of Problem A. Thus, the stress components cannot be determined from the values of stress invariants. (a) Problem A; (b) Problem B; (c) Problem C; (d) Problem D; (e) Problem E.

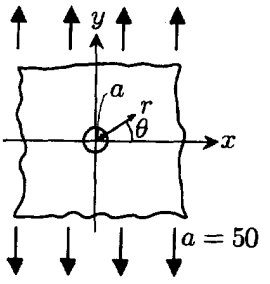

(a) Infinite plate containing a circular hole under tension.

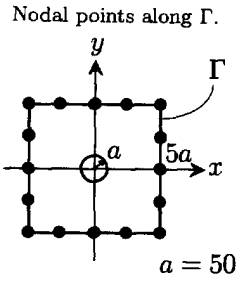

(b) Domain Γ for BEM analysis of (a) (Boundary of the circular hole is divided into 36 elements).

Fig. A2. In (a) an infinite plate is assumed to be a total structure. The domain with the boundary Γ in (b) is picked up from (a) to determine the stress components in the vicinity of the circular hole. (a) Infinite plate containing a circular hole under tension. (b) Domain Γ for BEM analysis of (a) (Boundary of the circular hole is divided into 36 elements).

APPENDIX B: ANALYTICAL DATA ON AN INFINITE PLATE CONTAINING A CIRCULAR HOLE UNDER REMOTE TENSION

In order to solve the problem of Fig. 3, a square region Ω of Fig. A2(b) is taken from Fig. A2(a). Γ is the boundary of Ω and is equally divided as shown in Fig. A2(b). The optimum stress to be distributed along Γ was determined by the proposed method using a commercial BEM program (Hirai, 1984). Table A1 shows the coordinates of the points where J_{1j} ($i = 1 \sim 56$) were adopted. The exact values of J_{1i} were calculated by eqn (6) as explained in the main text.

Table A1. Internal points where the values of J_1 were adopted in Fig. A2(b)

No.	x,	y	No.	x,	y	No.	x,	y	No.	x,	y
1	60,	0	15	80,	30	29	−100,	10	43	−40,	−50
2	70,	0	16	100,	30	30	−60,	30	44	−60,	−50
3	80,	0	17	40,	50	31	−80,	30	45	−80,	−50
4	0,	70	18	60,	50	32	−100,	30	46	−100,	−50
5	0,	80	19	80,	50	33	−40,	50	47	60,	−10
6	0,	90	20	100,	50	34	−60,	50	48	80,	−10
7	0,	120	21	−60,	0	35	−80,	50	49	100,	−10
8	120,	120	22	−70,	0	36	−100,	50	50	60,	−30
9	120,	100	23	−80,	0	37	−60,	−10	51	80,	−30
10	120,	0	24	−120,	120	38	−80,	−10	52	100,	−30
11	60,	10	25	−120,	100	39	−100,	−10	53	40,	−50
12	80,	10	26	−120,	0	40	−60,	−30	54	60,	−50
13	100,	10	27	−60,	10	41	−80,	−30	55	80,	−50
14	60,	30	28	−80,	10	42	−100,	−30	56	100,	−50

APPENDIX C: MESH PATTERN FOR 3D PROBLEM

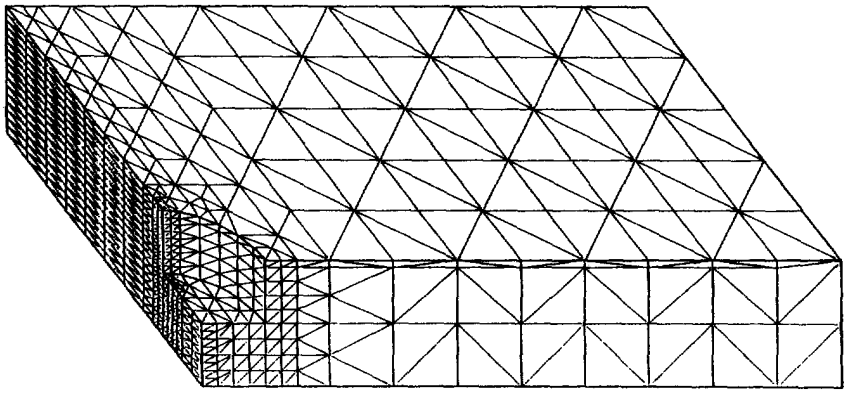

Fig. A3. Finite element meshing of the plate of Fig. 4.

Table A2. Analytical results of Fig. A3 [MPa]

(x, y, z) [mm]	J_1		σ_x	σ_y	σ_z
	Meas.	Cal.	Cal.	Cal.	Cal.
(0.375, 5.250, 5.917)	41.5	35.9	30.0	5.7	0.2
(0.375, 11.250, 5.917)	26.7	29.6	28.0	1.8	−0.1
(0.188, 0.563, 2.906)	34.8	28.6	26.0	2.6	0.1

Meas.: Measured stress Cal.: Calculated stress

APPENDIX D: INFLUENCE OF SPECIMEN SIZE ON THE MEASUREMENT AND ANALYTICAL RESULTS

Before the present study, a preliminary experiment was carried out using a smaller specimen. The shape was geometrically similar but the dimension is 3/10. Due to the limitation of the spatial resolution of the analyzer, the error in the analytical results was large.

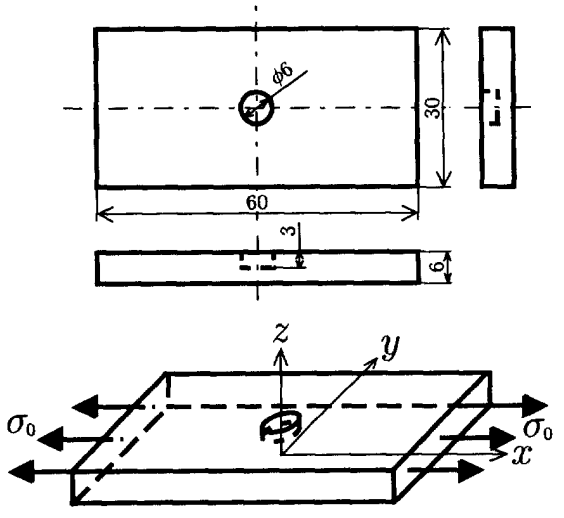

Fig. A4. Three dimensional problem (small specimen).